**Proceedings of the ASME 2020**
**International Mechanical Engineering Congress and Exposition**
**IMECE 2020**
**November 15 19, 2020, Portland, USA**

**PaperID**

# BEAM HARDENING ARTIFACT REDUCTION IN X-RAY CT RECONSTRUCTION OF 3D PRINTED METAL PARTS LEVERAGING DEEP LEARNING AND CAD MODELS

**Amirkoushyar Ziabari**[1,2] *

1. Imaging, Signals and Machine Learning
2. Manufacturing Demonstration Facility
Oak Ridge National Laboratory
Oak Ridge, TN
Email: ziabariak@ornl.gov

**Singanallur Venkatakrishnan** [1]
**Michael Kirka** [2,3]
**Paul Brackman**[2,4]
**Ryan Dehoff**[2,3]
**Philip Bingham** [1]
**Vincent Paquit** [1,2]

3. Deposition Science and Technology
Oak Ridge National Laboratory
Oak Ridge, TN
4. Carl Zeiss, Industrial Metrology LLC
Knoxville, TN

## ABSTRACT

*Nondestructive evaluation (NDE) of additively manufactured (AM) parts is important for understanding the impacts of various process parameters and qualifying the built part. X-ray computed tomography (XCT) has played a critical role in rapid NDE and characterization of AM parts. However, XCT of metal AM parts can be challenging because of artifacts produced by standard reconstruction algorithms as a result of a confounding effect called "beam hardening." Beam hardening artifacts complicate the analysis of XCT images and adversely impact the process of detecting defects, such as pores and cracks, which is key to ensuring the quality of the parts being printed. In this work, we propose a novel framework based on using available computer-aided design (CAD) models for parts to be manufactured, accurate XCT simulations, and a deep-neural network to produce high-quality XCT reconstructions from data that are affected by noise and beam hardening. Using extensive experiments with simulated data sets, we demonstrate that our method can significantly improve the reconstruction quality, thereby enabling better detection of defects compared with the state of the art. We also present promising preliminary results of applying the deep networks trained using CAD models to experimental data obtained from XCT of an AM jet-engine turbine blade.*

## 1 INTRODUCTION

X-ray computed tomography (XCT) involves taking x-ray images of a sample at different angles (see Fig. 3), normalizing the images, and computationally processing them using an algorithm to obtain a 3D reconstruction. The most commonly used algorithms make the assumption that the normalized data is linearly related to the unknown 3D object—an assumption that is valid when the x-ray source is monochromatic or when the sample is made up of relatively lighter elements if the source is polychromatic. In practice, however, the lower-energy photons in a polychromatic beam are absorbed more easily than the

*Address all correspondence to this author. This manuscript has been authored by UT-Battelle LLC under contract DE-AC05-00OR22725 with the US Department of Energy (DOE). Research was sponsored by the US Department of Energy, Office of Energy Efficiency and Renewable Energy, Advanced Manufacturing Office and by the Office of Nuclear Energy. 

higher-energy photons, which *harden* the x-ray spectrum as it passes through the object. This effect, called "beam hardening" [1], breaks the fundamental assumption of linearity implicit in common XCT reconstruction algorithms, thereby causing artifacts such as cupping (lower values for the reconstruction in the central regions) and streaking in reconstructed XCT images (see Fig. 1a). This phenomenon is more prominent for high-density materials such as metals, which are primarily used in metal additive manufacturing (AM) applications such as printing turbine blades for the aviation industry [2–5]. Beam hardening–induced artifacts make inference tasks such as detecting pores much more complicated; therefore, there is a need for fast algorithms and methods to handle such data.

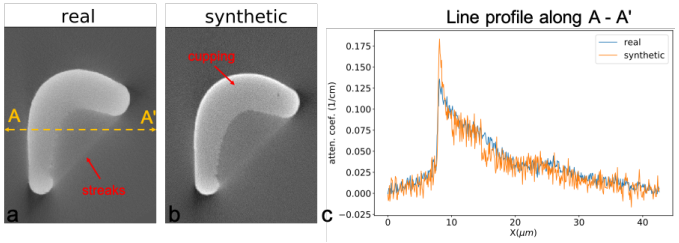


**FIGURE 1**. Cross section from the reconstruction of a jet engine turbine blade reconstructed using a standard reconstruction algorithm without accounting for beam hardening. The streaks and cupping artifacts (shown with red arrows) in the image can confound further analysis of the image to detect defects. Due to the cupping artifact, the reconstructed attenuation coefficient values of the part are non-uniform despite the fact that we scanned a homogeneous material. The reconstructed image is brighter at the edges (increased gray-level values), and are darker within the central region of the part (lower gray-level values). (a) From a real x-ray CT measurement (acquired by ZEISS METROTOM x-ray CT scan); (b) simulated blade; (c) Line-profile along central horizontal (A - A').

The topic of beam hardening and how to deal with it has been studied for several decades, dating back to the development of XCT itself [6]. One approach to dealing with beam hardening is to physically filter out the low energies of the x-ray spectrum [7, 8] using a filter and then reconstruct the data using standard algorithms. However, this hardware-based approach requires the manufacturing of well-calibrated filters that depend on the x-ray source spectrum and the materials being scanned. Furthermore, such filters lower the overall flux of the source, thereby increasing scan times or lowering the signal-to-noise ratio of the data. Another popular set of approaches involves the design of novel *algorithms* to computationally suppress artifacts that emerge as a result of beam hardening. These approaches can be broadly classified as those applicable to single-material and those applicable to multi-material samples. For single-material cases, one class of approaches involves designing a calibration sample of the same material as the object of interest and teaching a digital filter (such as a polynomial) to transform the data, effectively linearizing the data and then processing the linearized data using a standard reconstruction algorithm [1, 6]. Such a digital filter can also be empirically determined by finding the polynomial that, when applied to the projections, results in a visually pleasing tomographic reconstruction [9]. For samples composed of multiple materials, several algorithms have been developed that involve identifying the regions of different materials and correcting for each of these separately [10–13]. For the purposes of this paper, we focus on single-material samples, which are quite common in metal AM.

Recently, there has been work on developing deep learning–based techniques to address beam hardening artifacts. The authors in [14] use a U-Net to remove artifacts from the data itself by training on simulated pairs of mono-energetic and polychromatic data. The authors in [15, 16] address streak artifacts due to strongly attenuating materials embedded inside a larger object (a multi-material case) in the context of medical CT using a deep neural network (DNN) approach. [17] uses a data and image domain convolutional neural network (CNN) to remove metal artifacts in dental XCT (another example of the multi-material approach). The authors in [18] develop yet another approach for metal artifact reduction in medical CT. In summary, deep-learning approaches have recently emerged that show promising results for multi-material XCT mainly in the context of medical XCT.

In this work, we propose a novel framework based on using available CAD models for parts to be manufactured, accurate XCT simulations, and a DNN to produce high-quality XCT reconstructions from data that is affected by noise and beam hardening. In particular, we propose to use CAD models of the parts, introduce typical defects, and simulate XCT measurements that include a model for beam hardening and detector noise. These simulated measurements were processed with common XCT reconstruction algorithms, which resulted in artifacts. We then trained a deep learning model on the pairs of reconstructed volumes, with artifacts and ground truths derived from the CAD model, to learn a fast, nonlinear mapping function. The deep learning method will teach the model how to suppress the beam hardening artifacts and noise from the reconstructed volumes. Once the mapping is learned, the proposed deep learning method can rapidly process new data and produce reconstructions by effectively suppressing noise and beam hardening artifacts. In addition, the proposed DNN reconstructs a 3D volume using a *2.5D* scheme by which each slice is reconstructed from multiple slices of the input to exploit correlations between adjacent slices. This approach is in contrast to most deep learning approaches that either work with 2D images or are too expensive for use in processing entire 3D volumes. The proposed approach allows high-quality 3D reconstruction much faster than state-of-the-art methods. Using simulated and experimental data sets, we highlight the benefits of our proposed technique compared with existing approaches. Further we evaluate the proposed network, trained on synthetic data only, on experimental XCT data sets and demonstrate preliminary promising results in comparison with

standard reconstructions obtained from a commercial XCT system at the Manufacturing Demonstration Facility (MDF) at Oak Ridge National Laboratory (ORNL).

The rest of this paper is organized as follows. In section 2, we present details of our proposed deep learning–based algorithm. In section 3, we present the results of the use of our algorithm on realistic simulated data and experimental data. Conclusions are presented in section 4.

## 2 Proposed Approach for Simulation and Reconstruction

Our overall approach to addressing the challenge of beam hardening artifacts in XCT is given in Figure 2. We propose to use a CAD model of parts to be scanned, simulate realistic XCT data, and use this data, along with a DNN, to reconstruct the part accurately. Once such a deep-learning model has been trained, it can be applied to experimental data sets corresponding to the CAD models and obtain high-fidelity reconstructions.

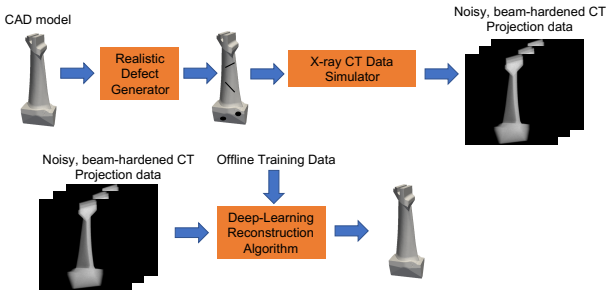


**FIGURE 2**. Concept of the the proposed solution to dealing with data sets impacted by beam hardening. Our method uses a CAD model, introduces realistic defects, and uses this model to simulate several realistic XCT data sets. We then design an algorithm aided by deep learning to accurately reconstruct the original 3D volume from such data. Once such a network has been trained, it can be applied to the experimental data for the part being scanned.

The simulation model is described in Sections 2.1 - 2.3, followed by a description of the DNN approach in Section. 2.4.

### 2.1 Conventional Cone-Beam CT

Figure 3 shows a schematic of a conventional cone-beam CT (CBCT) system typically used in industrial CT systems. A x-ray source (typically polychromatic) is used to illuminate the object of interest, and a corresponding transmission radiograph/image is obtained by a flat panel detector. To perform CT, the object is rotated about a single axis of rotation, and at each position, a projection image is measured. These measurements are typically normalized by a reference scan and then processed by an algorithm to obtain a 3D reconstruction. The most commonly used algorithm in commercial CT scanners is the Feldkamp-Davis-Kress (FDK) [19] method, which can analytically invert the measurements. The advantage of the FDK algorithm is that it is very fast, since it is based on an analytic expression that can be rapidly computed. However, the FDK method works best when a large number of projection images are measured and they provide a sufficiently high signal-to-noise ratio.

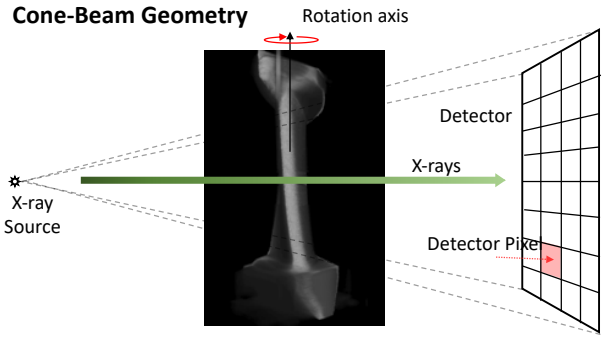


**FIGURE 3**. Schematic of a cone beam XCT system with a turbine blade as the object of interest. An x-ray source is used to illuminate an object of interest, and a detector measures the transmitted signal. The object is rotated, and several such measurements are made and processed by a tomographic reconstruction algorithm to produce a 3D reconstruction.

Another class of methods that has been widely researched for CT reconstruction are model-based image reconstruction (MBIR) approaches [20]. These MBIR algorithms work by formulating the tomographic reconstruction by minimizing a cost function that balances a data-fitting term. This term incorporates a physics-based model for the imaging system and noise characteristics of the detector, and a regularization term that incorporates a model for the underlying 3D object itself (such as local smoothness). MBIR techniques have enabled dramatic advances in several CT applications, including ultra–low-dose medical XCT, in which they have enabled high-quality reconstructions from sparse and extremely noisy data [21]. However, the use of MBIR for industrial CBCT is still in its infancy [22] because of the high computational demands dictated by the high-resolution detectors used in these applications. Furthermore, irrespective of the algorithm used, the aforementioned methods can result in reconstructions with significant artifacts if the underlying assumptions of the models used are violated, as is the case with beam hardening.

### 2.2 Simulation of XCT Data Using CAD Models

For a monochromatic source of x-rays at energy $E_0$, a common expression for the normalized measured signal is based on Beer-Lambert's law and is given by

$$-\log\left(\frac{I}{I_0}\right) = \mu_{E_0} d, \tag{1}$$

where $I$ is the attenuated intensity, $I_0$ is the reference intensity with no object in between, $\mu_{E_0}$ is the attenuation coefficient

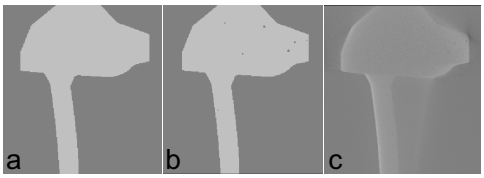


**FIGURE 4**. Illustration of our algorithm for creating realistic objects from the CAD model, simulating CT data, and reconstructing it using conventional algorithms that do not account for beam hardening. Cross section are shown from (a) the original CAD model, (b) a CAD model with defects, (c) a reconstructed CAD model with beam hardening and noise included in the simulations.

at energy $E_0$, and $d$ is the thickness of the material. In the case of a polychromatic source, $I$ and $I_0$ are related to the source spectrum ($f(E)$) and detector efficiency ($\gamma(E)$) through

$$I = \int e^{-\mu(E)d} f(E)\gamma(E)dE \tag{2}$$

$$I_0 = \int f(E)\gamma(E)dE. \tag{3}$$

Therefore, for a polychromatic light source, the linear relation between the normalized measurement and thickness ($d$) shown in Eq. (1) no longer holds. Although the expression in Eq. (2) is the most general form for x-ray transmission through a sample, using it for simulations requires knowledge of the source spectrum, the material attenuation coefficient as a function of energy, and the detector efficiency as a function of energy. Van de Casteele et al. [23] present a simplified bi-modal energy model that can accurately model the beam propagation using two dominant energies in the x-ray source beam. In such cases, and assuming the two dominant energies to be $E_1$ and $E_2$, one can write

$$-\log\left(\frac{I}{I_0}\right) = \mu(E_2)d + \log\left(\frac{1+\alpha}{1+\alpha e^{-(\mu(E_1)-\mu(E_2))d}}\right) \tag{4}$$

$$\alpha = \frac{f(E_1)\gamma(E_1)}{f(E_2)\gamma(E_2)}. \tag{5}$$

At the limit for small thicknesses ($d \to 0$), Eq. (4) reduces to

$$-\log\left(\frac{I}{I_0}\right) = \left(\frac{\alpha}{1+\alpha}\mu(E_1) + \frac{1}{1+\alpha}\mu(E_2)\right)d \equiv \mu_{eff}d, \tag{6}$$

which is same as Beer's law with an effective attenuation coefficient $\mu_{eff}$. The expression $\mu_{eff}$ is assumed to be the attenuation coefficient of the material if the x-ray source were monochromatic and therefore no beam hardening would have occurred. We used these parameters to model beam hardening and to generate synthetic data for the results in this paper.

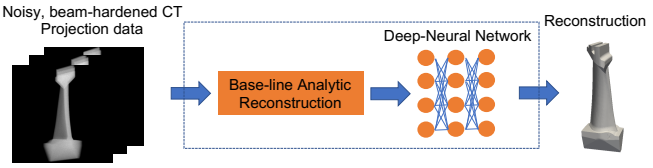


**FIGURE 5**. Illustration of the deep neural network architecture used in this paper. The first step is to invert the data using a standard algorithm, followed by use of a deep-neural network to remove artifacts due to noise, sparse sampling and beam hardening.

### 2.3 XCT simulations with Beam Hardening Using CAD Models

To simulate XCT reconstruction from beam hardened measurements, we used the CAD models of a part to be scanned using XCT once it has been manufactured. The process for creating a synthetic data set is as follows:

1. We estimated $E_1$, $E_2$, and $\alpha$ for the system and sample to be scanned. This procedure is briefly outlined at the end of this list.
2. We voxelized the CAD model corresponding to the sample to be scanned and interpolated it to the desirable resolution. An example cross section of half a blade is shown in Figure 4a.
3. We generated volumes with defects of different shapes and sizes. Cracks, holes/pores were the main defects simulated. For crack propagation in 2D layers, we assumed polynomials with fractional exponents that are randomly chosen between 0.7 and 1.2 at different locations throughout the 3D volume. The pores/holes were selected to be between 1 and 9 pixels in diameter, randomly distributed along the volume.
4. We performed logical And operation between the CAD model and the defect volume (Figure 4b). Half the volumes were blurred with a Gaussian filter, so that the defects do not look sharp, small defects become faded, and the model becomes more realistic (Figure 4b).
5. We simulated a typical XCT scan of the part with parameters relevant to our system and calculated the simulated projection data for the blades. In this simulation, we used the ASTRA toolbox [24, 25] for forward projection, modified to account for beam hardening using Eq. (4), and simulated Poisson statistics for the measurement.
6. We reconstructed the volume using the FDK algorithm [19] from ASTRA toolbox [24,25]. A cross section of the reconstructed volume presented in (Fig. 4c) clearly shows beam hardening artifacts such as cupping and streaks.

To obtain realistic-looking synthetic data, we used experimental projection data from a 3D printed part (Inconel738 material in our case), and fitted $E_1$, $E_2$, and $\alpha$ so that the reconstructions obtained from the simulated data matched the one obtained from the real XCT measurement of the blade. See Figure 1 for a comparison of cross sections of the reconstruction along the airfoil region created from synthetic and from experimental data.

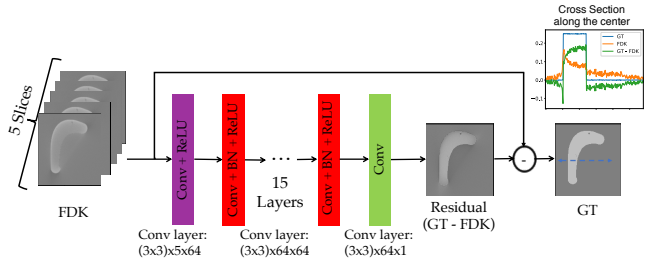


**FIGURE 6**. Schematic of the deep residual neural network architecture (AI-CT). The network learns to predict the residual artifacts and noise from the low-quality input reconstruction, which can then be subtracted from the input to approximate a reconstruction close to the high-quality ground truth.

### 2.4 Deep Learning–Based Beam Hardening Correction

The goal of beam hardening correction algorithms is to suppress artifacts in the 3D CT reconstruction. In additive manufacturing this allows one to accurately characterize the parts; develop statistical models that can find the correlation between printing parameter, scan path, and so on with the characterization results; and then use that information to improve the quality and consistency of the parts being built. In this section, we propose a deep learning–based method to suppress noise and beam hardening artifacts in the reconstructed volumes. Our overall approach is illustrated in Figure 5. It involves obtaining an initial reconstruction using the FDK [19] algorithm, followed by using a DNN to correct for the beam hardening artifacts present in the 3D volume. The DNN suppresses noise and artifacts in the 3D volume based on parameters learned from an offline training stage. There are several options from which to choose a DNN. This paper compares two different architectures— AI-CT [26, 27], and MSD-Net [28, 29], which has been used to remove conventional noise from CT reconstructions.

The following are key points regarding the network and the training process:

1. The schematic of AI-CT is shown in Figure 6. It consists of 17 convolutional layers with the transformation kernel of the form $(3 \times 3) \times N_{in} \times N_{out}$. Here, $(3 \times 3)$ represents the convolution filter size applied with $N_{in}$ input and $N_{out}$ output channels. Batch normalization (BN) and ReLU were applied in the middle 15 layers.
2. The MSD-Net was comprised of an 80 layer mixed-scale dense neural network, with 8 levels of dilation in the filters. The filters were chosen to be of size $3 \times 3$. We used a batch size of 1 for training the neural network.
3. The input pairs used in training the network were the 3D volume of the FDK image reconstruction of the same blade with beam hardening artifacts and noise, and the ground-truth volume with the effective attenuation coefficient and with a small additive Gaussian noise. We found that adding this small amount of noise to the "perfect" CAD models helped in improving the performance of the network on experimental data sets (generalization). For AI-CT, the network was trained on pairs of noisy input and the residual output, i.e., the difference between the expected output and the input. For MSD-Net, the network was trained on pairs of noisy input and the CAD-based ground truth.
4. In the case of AI-CT, we trained the network on patches of data from the input volumes. The input patches were of size $n \times n \times 5$, where $n$ was chosen to be 256. The number of neighboring slices was chosen to be five, based on the analysis in ref. [27], which demonstrated that such approach allows the network to capture the 3D information in a 2.5D fashion, which in turn increases the accuracy without adding computational burden. We used a batch size of 16 for training the neural network. For MSD-Net, also, the number of adjacent slices was set to 5. In contrast to the AI-CT network, MSD-Net was trained on the entire image instead of chunking it into patches. Here, we used a batch size of 1 for training the neural network.
5. We used a mean-squared error criterion to train the neural networks. For both networks, an ADAM optimizer minimized the loss function with $\alpha = 0.001$, $\beta_1 = .9$ and $\beta_2 = 0.999$. In AI-CT, the learning rate reduces by a factor of 2X every 70 epochs, or if the validation loss increases for three consecutive epochs, whichever happens first.
6. We trained the proposed networks on six volumes of CT reconstructions. These volumes were from three blades with different artifacts and different noise levels, different blurring, but the same beam hardening parameters. For the AI-CT method, the input volumes were divided into patches of data to avoid memory problems and to enable the use of more input data [27, 30]. We used a patch size of $256 \times 256$ with a stride of 128; thus, each slice (image from the 3D volume) of $768 \times 768$ was divided into $25 \times 256 \times 256$ patches (sub-images). In addition, patches with too many background voxels were removed (patches with average values smaller than the mean of the total volume) to improve training. Effectively, half of the volumes were used to create the training/validation data. We used 80% of those total patches for training and 20% for validation.
7. The same data was used to train the MSD-Net. A similar 80%/20% fraction of data was used for training and validation, but the data did not have to be patched, as the network operated on the entire image.

## 3 Results

### 3.1 Synthetic Data

**3.1.1 Conventional Techniques** Before discussing the results for deep learning–based methods, and for completeness of the work, we briefly discuss the results obtained using standard techniques such as FDK and MBIR to perform the reconstruction. One caveat regarding those techniques is that a calibration sample is needed to account for beam hardening and

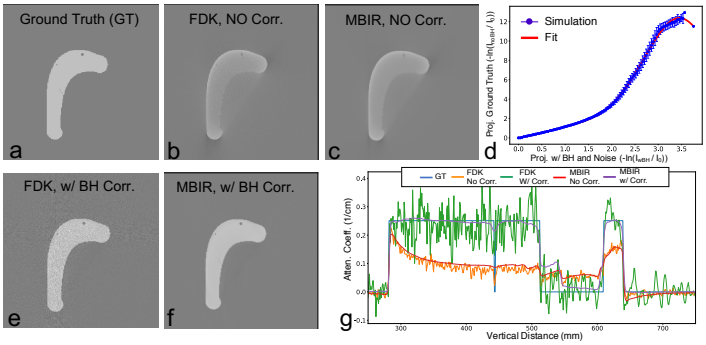


**FIGURE 7**. Linearization technique to remove beam hardening artifacts followed by the use of well known algorithms (FDK and MBIR). Using CAD model simulations allowed us to find a polynomial fit for linearization of projection data and in turn perform beam hardening correction in the projection domain.

to correct the projection data before performing reconstruction. The linearization approach of [1,6] finds a polynomial that maps the beam hardened projection to the projection without beam hardening—effectively linearizing the relationship between normalized measurement and sample thickness. Instead, we simulated the XCT system with a CAD model as object, obtained the projection data affected by beam hardening artifacts and noise ($\text{Proj}_{wBH}$), and obtained the projection data unaffected by beam hardening ($\text{Proj}_{NoBH}$) using the effective attenuation coefficient from Eq. (6). Next, we found the polynomial fit that mapped the projection values from $\text{Proj}_{wBH}$ to $\text{Proj}_{NoBH}$ (see Figure 7d).

We divided the interval between minimum and maximum projection values in the $\text{Proj}_{wBH}$ into a hundred equal parts. We found all the pixels that matched these values to the fourth decimal point, and then found the projection values for those voxels in $\text{Proj}_{NoBH}$. The mean of the projection values in $\text{Proj}_{NoBH}$ at those voxels is plotted against the values in $\text{Proj}_{wBH}$ in Figure 7d. We carried out a Cp analysis [31,32] for the zero to 11th-order fits of the data and found that an 8th-order fit must be used for this data; that finding matches what is suggested in ref [33]. The polynomial fit was then applied to each pixel in the $\text{Proj}_{wBH}$ data to create the corresponding corrected projection data. FDK and MBIR were used to perform the reconstruction of data with and without beam hardening correction. A slice from the reconstructed volume is shown for each method in Figure 7 b,c,e,f, and is compared with the ground truth in Figure 7 a. As expected, both FDK and MBIR produced accurate reconstructions with this linearization scheme to remove beam hardening. The MBIR technique was more effective in suppressing noise while preserving details in the reconstruction. We emphasize that this result is the best we can expect from FDK and MBIR in dealing with beam hardening because the ground-truth volume is being used with no beam hardening to perform linearization. The following section discusses the use of FDK with no correction (to show the impact of beam hardening) and MBIR with a corrected projection for comparison with deep learning techniques.

**3.1.2 Deep Learning–Based Methods** We tested AI-CT and MSD-Net (see Section 2.4) on volumes of CT data with different defect sizes and noise levels from those in the training. In particular, although we used the same algorithm described in Section 2.3 to generate defects, we further applied erosion morphological operations [34] to produce smaller defects than those for which the network was trained. This approach was used to evaluate its capability to reconstruct those defects. Note that for testing in AI-CT, we used full image slices as input to avoid artifacts due to patching.

The results for the reconstruction of two case studies between deep learning–based techniques and MBIR with beam hardening corrected projection are compared in Figures 8 and 9. In the comparison, the second case study is a volume with blurred defects, which make the reconstruction more challenging. Figure 8 shows a slice near the bottom of the reconstructed blade for case study 1. The reconstruction was performed using FDK (without correction), MBIR (with corrected projection, as in Figure 8), MSD-Net, and AI-CT. Three regions of interest that include such defects were chosen for comparison, as shown in Figure 8a. The results suggest that although both deep learning–based reconstruction techniques performed well, AI-CT picked up pores that were not clear in the other reconstructions. It also produced a sharper reconstruction when reconstructing the defects.

Figure 9 compares the methods for a more challenging case study in which the defects were blurred before modeling XCT and applying beam hardening. We selected two slices in the airfoil region (Figure 9a–e and 9f–j) and one slice near the bottom of the blades (bottom row, Figure 9k–o). Slices were selected specifically to make it challenging for all the algorithms to reconstruct the defects. For each case, the expanded views of the regions of interest are shown as insets for better comparison. Overall, AI-CT demonstrates consistent performance in reconstructing the XCT volume of data and removing the artifacts and noise while restoring the defects more accurately.

We further made a quantitative comparison among the methods along all the slices in the volume. We used the peak signal-to-noise- ratio (PSNR) as the main metric for the quantitative comparison. The PSNR is calculated using

$$PSNR \equiv 20\log\left(\frac{x_{GT,max}}{MSE}\right), \tag{7}$$

where mean squared error (MSE) is defined as $MSE \equiv \frac{1}{N}\sum_{i=1}^{N}(x_{GT}(i)-x(i))^2$, and $x_{GT,max}$ is the maximum pixel value in the ground-truth image. Here, $N$ is the total number of voxels, $x_{GT}$ is the voxel that belongs to the ground-truth volume, and $x$ is the corresponding voxel in the reconstructed volume. To avoid voxels in the air or background of the image slices, we used only voxels that were within the CAD model region of the part. The PSNR values for AI-CT outperformed the other methods by at least $4dB$, highlighting the strength of our proposed solution.

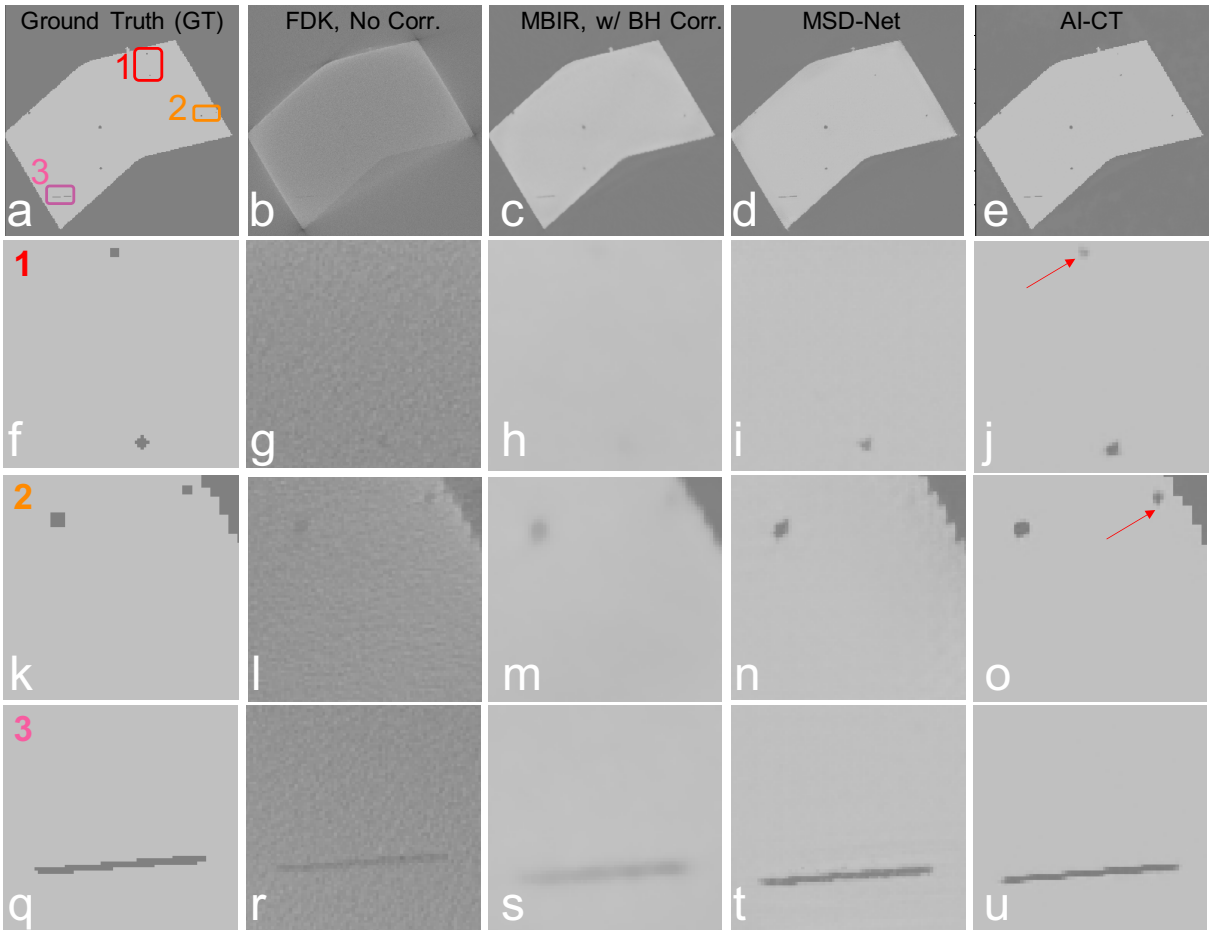


**FIGURE 8**. (Top row: (a-e) Comparison among different methods for a single slice in the reconstruction volume. Rows 2-4 (f-u) compare the results in the three regions of interest (1, 2, and 3) marked in panel a. Overall, AI-CT produces sharper reconstructions and identifies defects that are not visible in the other reconstructions (e.g., panels j and o) .

**TABLE 1**. Mean PSNR And SSIM for Reconstruction Volumes

| Method | FDK, No Corr. | MBIR w/ BH Corr | MSD-Net | AI-CT |
|---|---|---|---|---|
| Avg. PSNR (*dB*) (Case 1) | 16.42 | 36.52 | 37.24 | **53.11** |
| Avg. PSNR (*dB*) (Case 2) | 16.37 | 41.47 | 35.68 | **45.05** |

### 3.2 Synthetically Trained Networks for Real XCT Data

So far, we have simulated the XCT system and beam hardening effect using CAD models and shown that the trained neural networks, especially the proposed AI-CT method, produced sharp and accurate reconstructions of simulated test data sets. This section answers the following question: *How accurate are neural networks trained using synthetic data when applied to real XCT data volumes of the part corresponding to the training CAD models?* This is an important question, because acquiring and creating real labeled training data is labor intensive, expensive, and time consuming. Hence, having networks that are trained only on synthetic data and can be applied to real data would be invaluable. To answer the question and in turn identify the strengths and shortcomings of the trained networks, we tested the trained networks (MSD-Net and AI-CT) on a reconstruction of a turbine blade scanned at the MDF at ORNL using a ZEISS METROTOM XCT system. Results for some slices are shown in Figures 10 and 11. Figure 10 shows two cross sections of the reconstructed volume in the airfoil region of the blade. We compared the results for the deep networks with the standard output of the XCT system at the MDF. It is clear from Figure 11 that even though AI-CT was trained only on synthetic data, it does an excellent job of reconstructing the blade and identifying the defects and inclusions. On the other hand, MSD-Net was not able to recover the defects in reconstruction and introduced artifacts near the edges where beam hardening streaks existed. Note that these limitations could potentially be overcome by better tuning the hyper-parameters of MSD-Net during training. It should be emphasized that the networks are trained only on synthetic data, giving further significance to the importance of the results obtained.

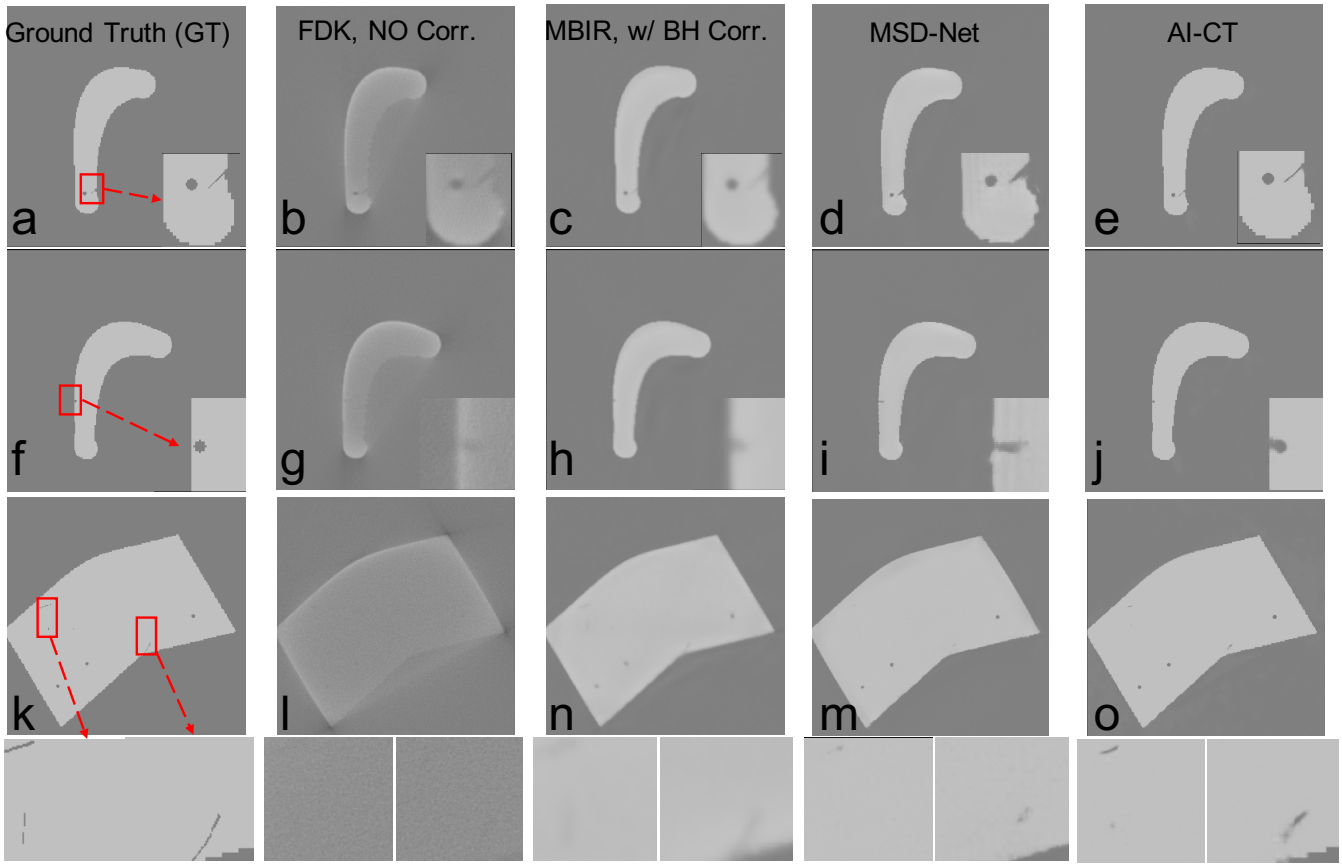


**FIGURE 9**. Comparison at slices in the airfoil region, (a–e) near center; (f–j) between center and bottom; and (k–o) near the bottom of the blade. The expanded views of the regions of interest are shown in the inset. The bottom row shows an example where all methods have difficulty in restoring the defects.

On the other hand, in Figure 11, it can be seen that some pores and defects appear in the reconstructed slices at the bottom of the blade using AI-CT. Since a ground truth for real data is not available, we cannot either repudiate those defects/holes as artificial features, or accept them as real defects not visible to standard techniques. Specifically, this is because AI-CT has already proved in Figure 8, j and o, that it is capable of identifying pores and defects that are not visible in other reconstructions. Therefore, further analysis, and maybe measurements with different modalities, are needed.

Based on these results, we leave the question asked above as open-ended, and defer answering it to future work. Nevertheless, we think the results documented in this paper are unique and a promising step in leveraging CAD models for more consistent and precise characterization of metal AM parts using XCT.

### 3.3 Discussions

Based on the results shown for both synthetic as well as real data sets, the key factors contributing to the significance of the proposed method are summarized as follows. First, removing/reducing beam hardening artifacts when dealing with XCT reconstruction of metal parts will increase the accuracy of characterization of the 3D printed parts. Accurate characterization beyond current state-of-the-art is beneficial in advancing statistical analysis of pores/defects/cracks in the manufactured parts, correlating them with 3D printing parameters, and in turn increase the efficacy and consistency of 3D printing process. Second, a fast and accurate deep learning–based technique is beneficial in streamlining the process of characterization of several hundreds of parts being manufactured and characterized every day at manufacturing centers such as the Manufacturing Demonstration Facility (MDF). Third, developing a deep learning method that is trained ”only” on synthetic data, and can be employed for testing and analysis of real data is a major challenge in artificial intelligence (AI) research domain. Our method will help significantly reduce the necessity of performing the cumbersome, labor-intensive and expensive task of curating real data sets for training a supervised deep learning network. Fourth, the modularity of the proposed technique provides a plug-and-play framework that can take any state-of-the-art CNN as a module, and perform a high quality XCT reconstruction of the 3D volume. Fifth, the proposed method helps in reducing the scan

time and cost for NDE of parts; using a shorter scan time results in a lower quality analytical reconstruction, and as shown throughout the results section, AI-CT is trained to approximate the high quality reconstruction taking the low quality reconstruction as input. Last, while the proposed technique is developed for characterization of metal parts, it can be extended to other areas such as medical imaging, nuclear engineering, security, etc.

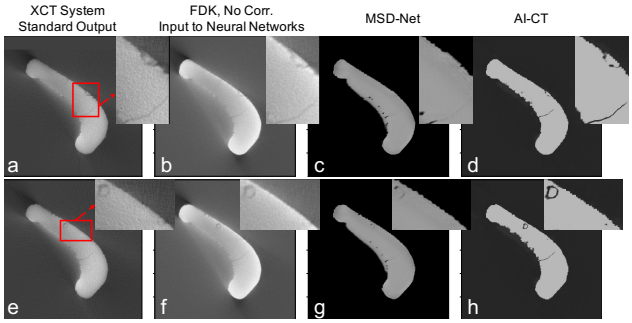


**FIGURE 10**. Significant performance of AI-CT in reconstruction of real data in the airfoil region. ***Both AI-CT and MSD-Net were trained only on synthetic data***.

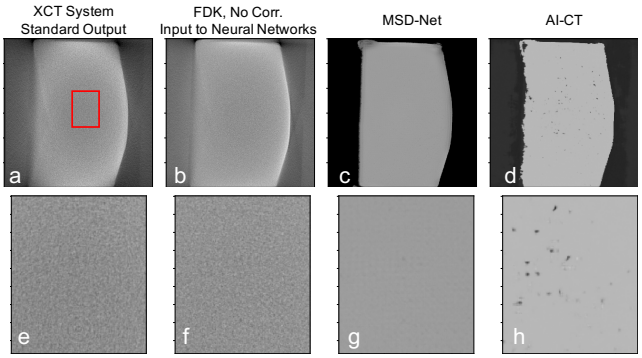


**FIGURE 11**. A reconstructed slice from the 3D volume that may show the limitations of neural networks trained on synthetic data only when they deal with real data sets. Considering the accuracy of the AI-CT results in Figure 8, j and o, further analysis and measurements are needed to evaluate the observed defects/pores in this figure, and in general, for real data.

## 4 Conclusion

Even after four decades of development, beam hardening still is an unresolved challenge for XCT of complex geometries of dense materials that are being used for metal AM. This paper showed how CAD models along with powerful DNNs can be leveraged to suppress beam hardening artifacts, such as cupping and streaks, in reconstructed XCT images. We used simulated XCT data with (and without) beam hardening and noise to train two separate deep CNNs, one that was developed by our team (AI-CT) and the state-of-the-art CNN MSD-Net. We evaluated the networks on different case studies with defects smaller than those generated in the training data sets. The test results demonstrated that AI-CT produces high-quality reconstructions that resolve these defects. In addition, we showed promising preliminary results for the reconstruction of experimental data sets, although AI-CT was trained only on synthetic data. This study paves the way for future development of DNNs that leverage CAD models for high-quality reconstruction and, in turn, enhanced nondestructive evaluation and characterization of complex 3D printed geometries.

## ACKNOWLEDGMENT

This research used resources of the Compute and Data Environment for Science (CADES) at Oak Ridge National Laboratory, which is supported by the Office of Science of the US Department of Energy under Contract No. DE-AC05-00OR22725. This research was supported by the Transformational Challenge Reactor program, US Department of Energy, Office of Nuclear Energy. S.V. Venkatakrishnan was supported by ORNL's AI Initiative Laboratory Directed Research and Development program.

## REFERENCES

[1] Brooks, R. A., and Di Chiro, G., 1976. "Beam hardening in X-ray reconstructive tomography". *Physics in medicine & biology,* ***21***(3), p. 390.

[2] Adair, D., Kirka, M., and Ryan, D., 2019. "Additive manufacture of prototype turbine blades for hot-fired engine performance validation trials". In ASME Turbo Expo 2019: Turbomachinery Technical Conference and Exposition, American Society of Mechanical Engineers Digital Collection.

[3] Lee, Y., Kirka, M. M., Ferguson, J., and Paquit, V. C., 2020. "Correlations of cracking with scan strategy and build geometry in electron beam powder bed additive manufacturing". *Additive Manufacturing,* ***32***, p. 101031.

[4] Kirka, M., Halsey, W., Rose, D., Ziabari, A., Paquit, V., Dehoff, R., and Brackman, P., 2020. "Analysis of data streams for qualification and certification of inconel 738 airfoils processed through electron beam melting". *Selected Technical Papers (STP), ASTM Symposium,* ***4***.

[5] Madara, S. R., and Selvan, C. P., 2017. "Review of recent developments in 3-d printing of turbine blades". *European Journal of Advances in Engineering and Technology,* ***4***(7), pp. 497–509.

[6] Herman, G. T., 1979. "Correction for beam hardening in computed tomography". *Physics in Medicine & Biology,* ***24***(1), p. 81.

[7] Xavier, M. S., Yang, S., Comte, C., Bab-Hadiashar, A., Wilson, N., and Cole, I., 2020. "Nondestructive quantitative characterisation of material phases in metal additive

manufacturing using multi-energy synchrotron x-rays microtomography". *The International Journal of Advanced Manufacturing Technology,* ***106***(5-6), pp. 1601–1615.

[8] Jennings, R. J., 1988. "A method for comparing beam-hardening filter materials for diagnostic radiology". *Medical physics,* ***15***(4), pp. 588–599.

[9] Kyriakou, Y., Meyer, E., Prell, D., and Kachelrieß, M., 2010. "Empirical beam hardening correction (EBHC) for CT". *Medical physics,* ***37***(10), pp. 5179–5187.

[10] De Man, B., Nuyts, J., Dupont, P., Marchal, G., and Suetens, P., 2001. "An iterative maximum-likelihood polychromatic algorithm for ct". *IEEE transactions on medical imaging,* ***20***(10), pp. 999–1008.

[11] Amirkhanov, A., Heinzl, C., Reiter, M., Kastner, J., and Groller, E., 2011. "Projection-based metal-artifact reduction for industrial 3d X-ray computed tomography". *IEEE Transactions on visualization and computer graphics,* ***17***(12), pp. 2193–2202.

[12] Jin, P., Bouman, C. A., and Sauer, K. D., 2015. "A model-based image reconstruction algorithm with simultaneous beam hardening correction for X-ray CT". *IEEE Transactions on Computational Imaging,* ***1***(3), pp. 200–216.

[13] Champley, K., and Bremer, T., 2014. Efficient and accurate correction of beam hardening artifacts. Tech. rep., Lawrence Livermore National Lab.(LLNL), Livermore, CA (United States).

[14] Pauwels, R., Cao, W., Wang, B., Xiao, Y., and Dewulf, W., 2019. "Exploratory research into reduction of scatter and beam hardening in industrial computed tomography using convolutional neural networks". In 9th International Conference on Industrial Computed Tomography, Location: Padova.

[15] Zhang, Y., and Yu, H., 2018. "Convolutional neural network based metal artifact reduction in X-ray computed tomography". *IEEE transactions on medical imaging,* ***37***(6), pp. 1370–1381.

[16] Ghani, M. U., and Karl, W. C., 2018. "Deep learning based sinogram correction for metal artifact reduction". *Electronic Imaging,* ***2018***(15), pp. 472–1.

[17] Lee, D., Park, C., Lim, Y., and Cho, H., 2019. "A metal artifact reduction method using a fully convolutional network in the sinogram and image domains for dental computed tomography". *Journal of digital imaging*, pp. 1–9.

[18] Gjesteby, L., Yang, Q., Xi, Y., Zhou, Y., Zhang, J., and Wang, G., 2017. "Deep learning methods to guide CT image reconstruction and reduce metal artifacts". In Medical Imaging 2017: Physics of Medical Imaging, Vol. 10132, International Society for Optics and Photonics, p. 101322W.

[19] Feldkamp, L. A., Davis, L. C., and Kress, J. W., 1984. "Practical cone-beam algorithm". *Josa A,* ***1***(6), pp. 612–619.

[20] Bouman, C. A., 2013. *Model Based Image Processing*.

[21] Pickhardt, P. J., Lubner, M. G., Kim, D. H., Tang, J., Ruma, J. A., del Rio, A. M., and Chen, G.-H., 2012. "Abdominal ct with model-based iterative reconstruction (mbir): initial results of a prospective trial comparing ultralow-dose with standard-dose imaging". *American journal of roentgenology,* ***199***(6), pp. 1266–1274.

[22] Balke, T., Majee, S., Buzzard, G. T., Poveromo, S., Howard, P., Groeber, M. A., McClure, J., and Bouman, C. A., 2018. "Separable models for cone-beam mbir reconstruction". *Electronic Imaging,* ***2018***(15), pp. 181–1.

[23] Van de Casteele, E., Van Dyck, D., Sijbers, J., and Raman, E., 2002. "An energy-based beam hardening model in tomography". *Physics in Medicine & Biology,* ***47***(23), p. 4181.

[24] van Aarle, W., Palenstijn, W. J., Beenhouwer, J. D., Altantzis, T., Bals, S., oost Batenburg, K. J., and Sijbers, J., 2015. "The ASTRA toolbox: A platform for advanced algorithm development in electron tomography". *Ultramicroscopy,* ***157***(Supplement C), pp. 35 – 47.

[25] van Aarle, W., Palenstijn, W. J., Cant, J., Janssens, E., Bleichrodt, F., rei Dabravolski, A., Beenhouwer, J. D., Batenburg, K. J., and Sijbers, J., 2016. "Fast and flexible X-ray tomography using the ASTRA toolbox". *Opt. Express,* ***24***(22), Oct, pp. 25129–25147.

[26] Ziabari, A., Kirka, M., Paquit, V., Bingham, P., and Venkatakrishnan, S., 2019. "X-ray ct reconstruction of additively manufactured parts using 2.5 d deep learning mbir". *Microscopy and Microanalysis,* ***25***(S2), pp. 376–377.

[27] Ziabari, A., Ye, D. H., Srivastava, S., Sauer, K. D., Thibault, J.-B., and Bouman, C. A., 2018. "2.5 d deep learning for ct image reconstruction using a multi-gpu implementation". In 2018 52nd Asilomar Conference on Signals, Systems, and Computers, IEEE, pp. 2044–2049.

[28] Pelt, D. M., and Sethian, J. A., 2018. "A mixed-scale dense convolutional neural network for image analysis". *Proceedings of the National Academy of Sciences,* ***115***(2), pp. 254–259.

[29] Pelt, D. M., Batenburg, K. J., and Sethian, J. A., 2018. "Improving tomographic reconstruction from limited data using mixed-scale dense convolutional neural networks". *Journal of Imaging,* ***4***(11), p. 128.

[30] Lee, H., Lee, J., Kim, H., Cho, B., and Cho, S., 2018. "Deep-neural-network based sinogram synthesis for sparse-view ct image reconstruction". *arXiv preprint arXiv:1803.00694*.

[31] Mallows, C. L., 2000. "Some comments on cp". *Technometrics,* ***42***(1), pp. 87–94.

[32] Mallows, C. L., 1995. "More comments on cp". *Technometrics,* ***37***(4), pp. 362–372.

[33] Hammersberg, P., and Mångård, M., 1998. "Correction for beam hardening artefacts in computerised tomography". *Journal of X-ray Science and Technology,* ***8***(1), pp. 75–93.

[34] Gonzales, R. C., and Woods, R. E., 2002. Digital image processing.